

Tailoring optical and electrical properties of MgO thin films by 1.5 MeV H⁺ implantation to fluences

A. Moses Ezhil Raj^{a,*}, T. Som^b, V. Ganesan^c, M. Jayachandran^d,
G. Selvan^e, V. Swaminathan^f, C. Sanjeeviraja^g

^a Department of Physics, Scott Christian College (Autonomous), Nagercoil 629 003, India

^b Ion Beam Laboratory, Institute of Physics, Bhubaneswar 751 005, India

^c Low Temperature Laboratory, UGC-DAE CSR, Indore 452 017, India

^d ECMS Division, Central Electrochemical Research Institute, Karaikudi 630 006, India

^e Department of Physics, Thanthai Hans Roever College, Perambalur 621 212, India

^f School of Materials Science and Engineering, Singapore 639 798, Singapore

^g Department of Physics, Alagappa University, Karaikudi 630 003, India

Received 4 January 2008; received in revised form 28 February 2008

Available online 15 March 2008

Abstract

Thin films of magnesia (MgO) with (100) dominant orientations were implanted with 1.5 MeV H⁺ ions at room temperature to various fluences of 10¹³, 10¹⁴ and 10¹⁵ ions/cm². X-ray analysis unambiguously showed crystallinity even after a peak damage fluence of 10¹⁵ ions/cm². Rutherford backscattering spectrometry combined with ion channeling (RBS/C) was used to analyze radiation damages and defect distributions. Optical absorption band observed at 5.7 eV in implanted films was assigned to the anion vacancies and the defect was completely disappeared on annealing at 450 °C. Number of F-type defects estimated was 9.42 × 10¹⁵ cm⁻² for the film implanted with 10¹⁵ ions/cm². DC electrical conductivity of 4.02 × 10⁻⁴ S cm⁻¹ was observed in the implanted region which was three orders higher than the as-deposited films. In unison, film surface was modified as a result of the formation of aggregates caused by the atomic mixing of native matrix atoms (Mg and O) and precipitated hydrogen.

© 2008 Elsevier B.V. All rights reserved.

PACS: 77.55.+f; 78.66.Nk; 78.70.-g; 78.20.-e; 72.20.-i

Keywords: Thin films; Insulator; Implantation; Optical property; Electrical conductivity

1. Introduction

The effects of ion implantation in oxide ceramics have been extensively studied in the last few years, for a variety of ions, fluences and energies to modify the near-surface structure of crystalline solids. Among the oxides studied, MgO is a very stable oxide that can be used in a large range of technological applications. High stability makes it a suit-

able candidate to allow the controlled formation of colloidal dispersions of metallic precipitates using ion implantation [1–3]. Most of the physical properties exhibited by metallic nanoparticles embedded in two dimensional dielectric matrices are intriguingly different from those of the respective bulk material and may thus provide new optical and electrical properties [4]. Among the many possible ways, ion implantation is a very powerful technique to introduce nanoparticle clusters that modify the physical and chemical properties of the near surface region of dielectric films. These outstanding properties occur due to quantum size effects and the large surface area of the introduced nano-particles compared with their bulk counterparts [5–9].

* Corresponding author. Tel.: +91 04652 232888; fax: +91 04652 229800.

E-mail address: ezhilmoses@yahoo.co.in (A. Moses Ezhil Raj).

Under ion implantation, electronic excitation (electronic stopping) in insulators may cause atomic displacements, such as stimulated atomic desorption and ionization enhanced diffusion [10–12]. Such transitions in MgO thin films introduce stable vacancies and interstitials in the anion sub-lattice also. The defects induced by ion implantation have been monitored by optical absorption measurements based on defect creation [13]. The size of the formed nanoclusters depends on the full width at half maximum (FWHM) of the absorption band as a result of Mie plasmon resonance [14]. Likely by applying ion beam implantation, the electrical conductivity of crystalline oxides can often be increased by many orders of magnitude caused by defects, amorphisation, phase transformation and doping [15].

A number of implantation studies on single crystals of magnesium oxide have been performed using different analyzing techniques theoretically [16–19] and experimentally [20–23]. In this paper, we report on the effect of high energy (1.5 MeV) H^+ ions on MgO thin films forming small metal precipitates in their matrix. We combine X-ray diffraction (XRD), Rutherford backscattering spectrometry (RBS) to investigate the effects of implanted hydrogen on modifying the optical and electrical properties of insulating magnesium oxide thin films.

2. Experimental

MgO thin film samples were prepared using an indigenously assembled downward spray pyrolysis setup by optimizing the deposition conditions. Detailed informations regarding the experimental arrangement and the optimized deposition parameters were explained in our earlier report [24]. During implantation, hydrogen ions were accelerated in 9 SDH-2, NEC, 3 MV accelerator and made to fall on $1 \times 1 \text{ cm}^2$, $0.49 \text{ }\mu\text{m}$ thick MgO thin films for different fluences 10^{13} , 10^{14} and 10^{15} H^+ ion/ cm^2 at room temperature. The beam current was maintained low at nA range to avoid premature formation of clusters due to the ion beam heating of the MgO thin films. Required fluences ' F ' were calculated from the number of counts recorded in the monitor using the following equation:

$$F = \left(\frac{I}{qAq^+} \right) N, \quad (1)$$

where, ' I ' the current rating, ' q ' the electronic charge, ' A ' the implanted area, ' q^+ ' the charge state of the ion and ' N ' the number of counts. The projected range of 1.5 MeV H^+ ions have been estimated from TRIM simulations [19] and was in the μm range as estimated from the bulk density of MgO (3.582 g/cm^3).

X-ray diffraction patterns of the as-deposited and H^+ implanted films were recorded using an X'pert PRO diffractometer ($\Delta 2\theta = 10\text{--}70^\circ$, 0.2° as increment, integration time 1 s and Cu $K\alpha 1$ radiation, $\lambda = 1.5406 \text{ \AA}$). RBS and ion channeling were performed using 2.0 MeV alpha particles, at a 170° backscattered angle on MgO thin film samples. To limit channeling effects as far as possible, samples were

tilted during implantations by 7° relative to the normal direction. For this purpose, samples were mounted on a three axis precision goniometer, which allowed orientation with an accuracy of 0.05° . The analyzing particle beam from the accelerator was collimated to obtain a beam spot of 1 mm diameter with a divergence of less than 0.04° . To suppress secondary electrons, a ring-shaped electrode in front of the target was kept at a negative potential of 300 V. The optical absorption and transmission spectra were recorded in the wavelength range from 200 to 100 nm using a double beam spectrophotometer (Hitachi-3400). Electrical conductivity of these films was investigated in the temperature range $30\text{--}150^\circ\text{C}$ using the standard two probe technique. For measuring current, silver contacts were made onto two opposing lateral faces of the sample perpendicular to the large implanted face. The surface morphology of the films was investigated by atomic force microscopy (Nanoscope E – 3138J) in contact mode over a scan area of $150 \text{ }\mu\text{m} \times 150 \text{ }\mu\text{m}$.

3. Results and discussion

3.1. Structural modification

X-ray diffraction provides an extremely sensitive tool for detecting structural modifications and strains in implanted crystalline thin films. Since the diffracted intensity depends critically on lattice perfection, and therefore defects in the periodicity of the crystal lattice introduce imperfections that reduce the intensity. Further, introduction of dopant atoms into the lattice modifies the unit cell dimensions, crystallite size and also introduce strain. Preferentially (100) oriented MgO thin films deposited at 450°C were implanted with 1.5 MeV H^+ ions and then subjected to X-ray diffraction and the recorded spectra are shown in Fig. 1. Some disparity was observed before and after implantations in the diffraction spectra of the MgO samples. The X-ray diffraction pattern diagrams of as-deposited and implanted samples differ mainly on the peak intensities, full width at half maximum and positions of Bragg's peak. This variation of intensity is not decreased as a function of the diffraction angle and then cannot be explained only by an increasing of Debye–Waller factors. However, these variations can be explained on the basis of order–disorder transitions that occur during implantation. The driving force of this transition is induced by the energy deposited by electronic collisions that changes the crystallography of the material.

The order–disorder transition occurs mainly due to three reasons. Initially, the implanted hydrogen might be completely dissolved in the MgO lattice, replacing certain Mg atoms by the deformation of octahedral sites. This induces defect structure consisting of regions which deviate grossly from the original crystal lattice due to partial amorphisation or severe lattice distortions in the neighborhood of implanted precipitates. At low fluences disordered regions are created by collision cascades, recrystallize into

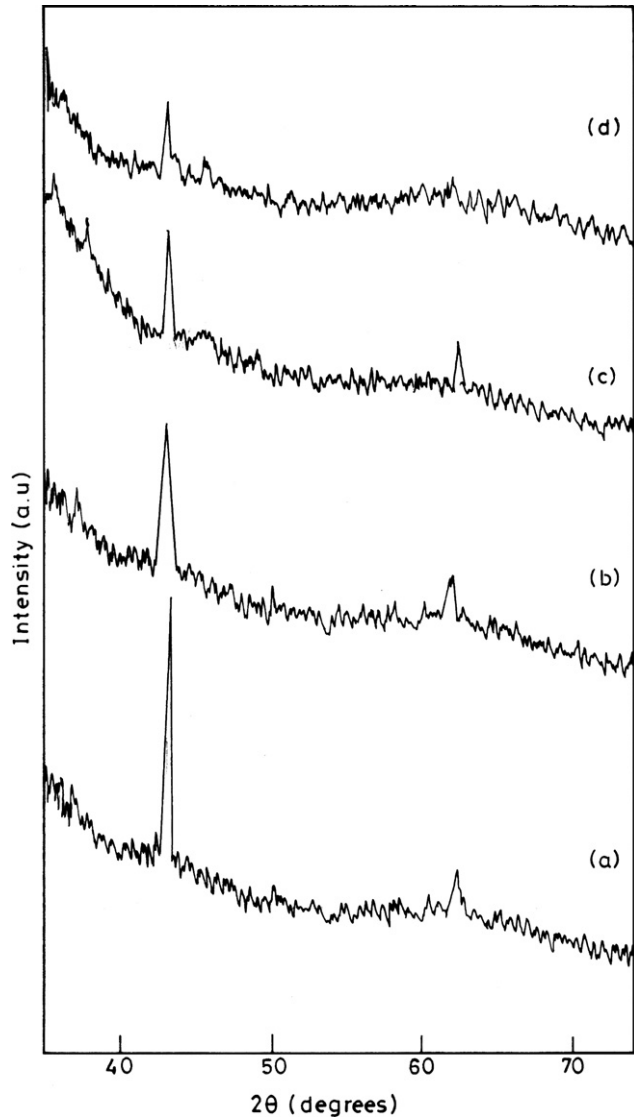


Fig. 1. XRD spectra of MgO thin films implanted with H^+ ions of various fluences: (a) as-deposited, (b) 10^{13} ions/cm², (c) 10^{14} ions/cm² and (d) 10^{15} ions/cm².

an imperfect lattice. However at high fluences, penetration of the implanted species that induces transition from perfect crystalline order leading to disordered amorphous nat-

ure. This is in accordance with results presented by Zimmerman et al. [25]. The recrystallization rate increases with increasing number of disordered regions, until equilibrium is attained. In addition to collision cascades, bombarding ions produced various defects along their paths and the slowed down H^+ ions formed O–H centers at lattice sites, giving origin to hole-trap centers and in turn reduce the crystalline nature of the lattice [26]. Finally, the bombarded H^+ ions sputtered some of the oxygen ions from the near surface region of the film causing deficiency in oxygen ions. This in turn causes disorderliness in the implanted crystal lattice.

As-deposited (unimplanted) MgO thin films have diffraction peaks corresponding to the diffraction angle 2θ at 42.78° and 61.85° and these peaks are corresponding to the reflecting planes (200) and (220) respectively (JCPDS Card No. 89-7746) [27]. The grain size calculated using the Scherrer formula [28] are respectively 29 nm and 18 nm for the (200) and (220) planes. On the implanted samples, the observed XRD peak intensity gradually decreases as the fluence is increased. This trend reveals that the crystalline nature of the implanted sample is reduced with rise in H^+ ion fluence. However, the structure is not modified, since all the characteristic lines of the Cubic fcc, $Fm\bar{3}m$ space group remain visible after implantations. However, vast deviations in interplanar d-spacings are observed and are listed in Table 1. The grain size [28], internal stress [29], microstrain [30], dislocation density [31] and density [32] are calculated using the measured values of full width at half maximum (β) of the diffraction peaks, unit cell dimension (a) and the diffraction angle (2θ). The internal stress is calculated by assuming the Young's modulus (286 GPa) [33,34] and Poisson's ratio (0.29) [35] values of the MgO single crystal. The average grain size of the MgO films implanted with hydrogen ions of fluence 10^{13} ions/cm² is less than that of the as-deposited samples. However, implanted samples with higher fluence 10^{14} and 10^{15} ions/cm² exhibit increased grain size. The internal stress and microstrain for the as-deposited and implanted samples along the dominant lattice orientation (200) are plotted in Fig. 2.

The internal stress for the as-deposited MgO sample is found to be tensile in nature. The stress may be due to

Table 1
Structural parameters of H^+ implanted MgO thin films

| Sample details | Diffraction angle (2θ) degree | hkl indices | Unit cell dimensions (a) (nm) | | FWHM ($^\circ$) | Grain size (D) (nm) | Internal stress (S) $\times 10^9$ (N/m ²) | Micro strain (ϵ) $\times 10^{-4}$ | Dislocation density (δ) $\times 10^{15}$ (lines/m ²) | Density (g/cm ³) |
|--|--|---------------|-----------------------------------|----------|-------------------|-------------------------|---|--|---|------------------------------|
| | | | Observed | Standard | | | | | | |
| As deposited (Unimplanted) | 42.78 | (200) | 0.4236 | | 0.301 | 29.60 | -1.99 | 8.5565 | 1.1407 | 3.52 |
| | 61.85 | (220) | 0.4238 | 0.4219 | 0.526 | 18.39 | -2.22 | 9.7763 | 2.9567 | |
| H^+ implanted 10^{13} ions/cm ² | 43.11 | (200) | 0.4196 | - | 0.4684 | 19.05 | 2.69 | 13.2017 | 2.7559 | 3.62 |
| | 62.42 | (220) | 0.4205 | - | 0.6528 | 14.86 | 1.64 | 11.9975 | 4.5268 | |
| H^+ implanted 10^{14} ions/cm ² | 43.15 | (200) | 0.4193 | - | 0.2676 | 33.35 | 3.04 | 7.5356 | 0.8993 | 3.63 |
| | 62.52 | (220) | 0.4199 | - | 0.9792 | 9.91 | 2.34 | 17.9602 | 10.1743 | |
| H^+ implanted 10^{15} ions/cm ² | 43.29 | (200) | 0.4180 | - | 0.2007 | 44.83 | 4.56 | 5.6318 | 0.5054 | 3.66 |
| | 64.41 | (220) | 0.4088 | - | 0.3672 | 26.71 | 1.53 | 6.4917 | 1.4019 | |

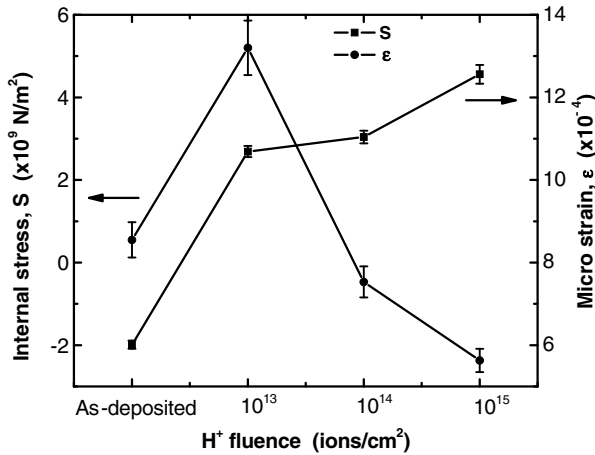


Fig. 2. Variation of internal stress and microstrain in MgO films implanted with H⁺ ions.

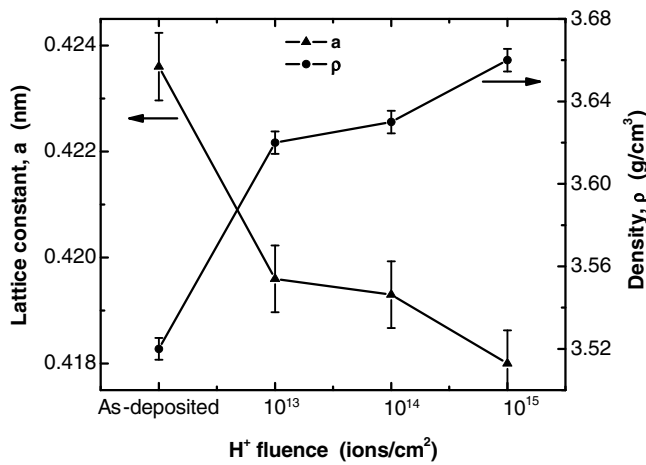


Fig. 3. Lattice constant and density variations in MgO films implanted with H⁺ ions.

the lattice misfit and it has a tendency to migrate parallel to the film surface so that the films have a tendency to expand and develop an internal tensile stress. For the implanted samples, internal stress is compressive that gradually increases with the fluence of implanted ions and this may be due to incorporation of the hydrogen ions in the MgO lattice. Ion implantation produces stresses that are usually compressive and biaxial in the plane of the sample surface. These findings are in agreement with the previously reported result [33]. The microstrain and dislocation density are decreased with increased fluence of ions. The lattice parameter and density variations with the fluence of hydrogen ions are shown in Fig. 3. The partial amorphous track produced during implantation compresses the crystalline area inducing macroscopic and microscopic strain fields in the sample. Upon implantation, atoms are displaced from their lattice sites and the cubic structure takes on a disordered appearance.

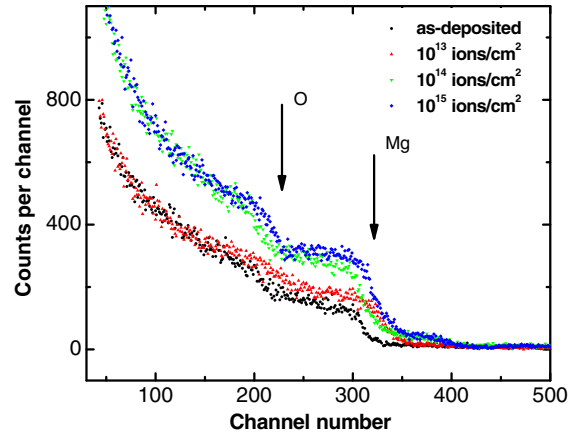


Fig. 4. Random RBS spectra recorded on MgO thin films implanted with 1.5 MeV, H⁺ ions at various fluences along with as-deposited sample.

3.2. RBS/C characterization

Channeling Rutherford backscattering spectrometry (RBS/C) is an important technique in characterizing the atomic disorder in crystalline materials [36]. However, its accuracy in the qualitative analysis of disorder profiles is limited by the ability to accurately deconvolute the signals contributed from two different scattering centers; one is the backscattering of channeled particles from displaced atoms and another is the backscattering of dechanneled particles from lattice atoms [37]. Deconvolution of the channeled particles were analyzed before and after ion bombardment. The beam divergence was set less than 0.1° with a spot size of 2 mm in diameter and beam current of about 10 nA, which was directly measured on the target. For random orientations, back scattering spectra of MgO thin films before and after implantation with H⁺ ions for different fluences are shown in Fig. 4. Figure reveals the microstructural changes in the implanted layers of the magnesium oxide thin films. The amount of disorder can be estimated for different elemental sub-lattices of the implanted thin films. The random spectrum obtained from the implanted films with less fluence exhibits less dechanneling than the highly implanted sample.

At lower fluences, near surface layer of the film samples are defect depleted. This is likely due to the migration of defects towards the surface of the crystal, which is a strong sink for defect annihilation. This effect is observed usually at grain boundaries of the polycrystalline samples that led to the suppression of the extended defects [38]. At higher fluences, one can note a significant extension of damage profile towards the sample depth. This extension of defect is attributed to defect diffusion, caused by the accumulation of radiation damages produced by the ions of large projected ranges [39]. In most of the studies performed, typical defects expected in implanted ceramics are amorphous clusters or dislocation loops [40,41]. At highest fluences, bubbles or colloids are created by implanted atoms

[42]. No such observations were noted for the present implantation fluences.

In order to measure the extent of the damage accumulation process, a commonly accepted parameter is the peak value of the radiation damage distribution (f_D^{\max}), defined as the normalized increase of the dechanneling yield [43]. In many oxide crystals implanted with moderate fluences, the accumulated defect $f_D < 1$. Within this limit, the defect accumulation does not lead to complete amorphisation of the crystal structure [44]. In the present study, the normalized dechanneling yield of 70% at high fluences agrees well with the previously reported results. This confirms that the lattice structure of MgO is destroyed to a lesser extent by H^+ implantation. This result is in agreement with the XRD results of the implanted layers. Complete amorphisation is not observed in the administered implanted fluences.

3.3. Optical absorption and transmission studies

Fig. 5 shows the optical absorption spectra of MgO thin films deposited on quartz substrates and implanted with H^+ ions for a fluence of 10^{15} ions/cm². After implantation, thermal annealing usually removes a great deal of lattice damage and therefore systematic investigations on the annealing behavior of implanted films have been carried out. Thermal annealing was performed in a tubular furnace in air at 450 °C for a period of 5 h. Absorption spectra of as-deposited and annealed samples after implantation are also given for comparison.

The absorption band observed in all the MgO thin film samples at 5 eV (~248 nm) corresponds to the presence of overlapping bands in the lattice due to 'F' and 'F⁺' centers. Other observed bands less intense at 5.7 eV (~217 nm) can be due to the anionic vacancies [45]. The absorption band occurred at 3.42 eV (~363 nm) can be assigned to the pairs of 'F' centers in nearest neighbor sites in anionic sub-lattice along (220) direction [46]. The broad absorption peak at 2.3 eV (~540 nm) is due to the presence of 'V' type centers

in the cationic sub-lattice [46]. The optical absorption band associated with metallic precipitate is observed at 560 nm, which is proportional to the number of hydrogen atoms in the metallic phase that decreases with annealing. Further, the optical measurements indicate that 'V' type defects annihilate completely at 450 °C, while the bands due to 'F' and 'F⁺' centers are annihilated partially at that temperature. However, Van Veen et al. [47] reported that most of the 'F' centers have disappeared on annealing at 275 °C.

From optical absorption measurements, the number of oxygen vacancies created by implantation can be estimated. The optical density (OD) of the F-type center band is related to the total number of defects ' N_F ' created per cm² of implanted surface by using Smakula's formula [46,48]:

$$N_F = \frac{0.87 \times 10^{17}}{f} \frac{n}{(n^2 + 2)^2} W_{1/2} (2.3 \text{ OD}), \quad (2)$$

where, ' n ' is the refractive index of film, ' $W_{1/2}$ ' is the band half width in eV and ' f ' is the oscillator strength.

For a particular defect center, the oscillator frequency ' f ' is constant and therefore the defect concentration depends on $W_{1/2}$ and OD. It is observed from Fig. 5 that the rate of intrinsic defect creation in the implanted sample is higher than the one observed in as-deposited MgO films. In the as-deposited MgO samples, the numbers of 'F' type centers are nearly 2.23×10^{15} cm⁻², whereas it increases to 9.42×10^{15} cm⁻² in the H^+ implanted samples. Refractive index $n = 1.73$ and the oscillator strength ' f ' of 0.8 were used to determine the number of defect centers ' N_F ' [49].

Further, in some of the MgO implanted samples to higher fluences, a light brown color tint was seen before annealing. This color change is caused by the implantation and occurred in the implantation zone. This color change affects the transmission properties of the films. The % transmittance of the H^+ implanted sample to a fluence of 10^{15} ions/cm² is shown in Fig. 6 along with the transmittance

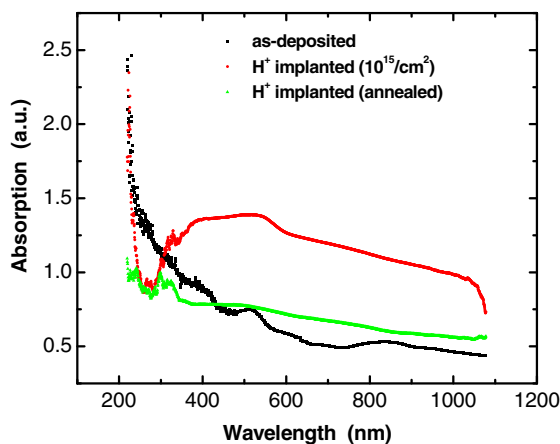


Fig. 5. Optical absorption spectrum of MgO thin films implanted with 1.5 MeV H^+ ions for the fluence 10^{15} ions/cm² along with spectra of as-deposited and annealed thin films.

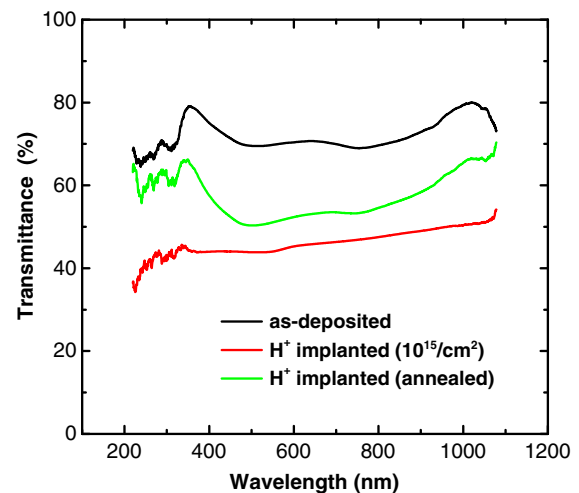


Fig. 6. Transmittance spectra of MgO thin films implanted with H^+ ions (10^{15} ions/cm²) along with as-deposited and post-annealed films.

tance spectra of as-deposited and post-annealed samples. The transmittance values are corrected relative to the optically identical uncoated substrate. The as-deposited MgO film has high transmittance $T > 70\%$ in the visible region. The sharp absorption edge in the low wavelength region (<300 nm) in the MgO film is attributed to the direct band gap. The absorption co-efficient is calculated to be 10^3 – 10^4 cm^{-1} based on the theoretical relation related to transmittance [50,51]. On implanted films, the optical transmittance is reduced to 45% in the visible region and it is increased to 52% on annealing at 450 °C for 5 h. However, the color tint appeared during implantation is completely vanished on annealing. The absorption edge shifts towards the long wavelength side on implantation with H^+ ions and this is true for the annealed sample also.

It has long been known that metallic colloids embedded in dielectrics produce colors associated with optical absorption [52–54]. This type of modification in the optical properties of insulating materials is seen in the implanted MgO films with MeV metal ions. Even after heat treatment, small metal clusters still remain in the implanted layer and absorb light [55–59]. The color change observed in the implanted layers thus modifies the refractive index of the MgO films.

The variation of refractive index (n) as a function of wavelength in the visible region is shown in Fig. 7. For theoretical comparison, a fit to Cauchy-type formula is made by multilinear regression method [60,61] using the formula,

$$n = 1.68366 + \frac{0.0184241}{\lambda^2} + \frac{5.1413 \times 10^{-4}}{\lambda^4}, \quad (3)$$

where, ' λ ' is in μm and the standard error of the above function is only 1.19×10^{-4} at the mean wavelength.

As seen from figure, the as-deposited MgO thin films have refractive index of about 1.81 ($\lambda = 500$ nm), which is in agreement with the bulk value of 1.73 [60] and with the regression fitting ($n = 1.76$), where as the implanted and annealed MgO films have refractive index slightly higher than the bulk value and have variations in the wave-

length region nearer to the 'F' center region. These variations can therefore be explained on the basis of annealing 'F' centers. In magnesium oxide, it is possible to anneal 'F' centers thermally. However, a fraction of vacancies is still stable. Further, implantation introduces vacancies, which causes expansion of the films. The number of 'F' centers formed is comparable to the molecular dilation. The 'F' band is thus a large band with high oscillator strength. Therefore, the F center causes an increase in refractive index in the visible region. In addition, from the increase of the refractive index, the characteristics of the 'F' peak can be measured. From its peak intensity and half-width relative to the 'F' peak, the rise in refractive index can be measured. Also, it is evident that the 'F' center peaks are in the visible spectral region [62].

3.4. Electrical characterization

Most of the insulators conduct ohmically below 0.1 MV/cm and this type of conduction is always extrinsic due to impurity, inhomogeneity, etc. Some insulators can behave as semiconductors when suitably doped with impurities or implanted with ions. Incorporation of these impurities in high concentration leads to a change in intrinsic behavior that changes the conduction type of the material. In the present study, the electrical conductivity of H^+ implanted magnesium oxide thin films have been studied. Using the two-probe technique, the dc electrical conductivity of MgO thin films implanted with 1.5 MeV hydrogen ions and fluences ranging from 10^{13} up to 10^{15} cm^{-2} has been recorded in the temperature range of 30 °C and 150 °C. The samples were not thermally annealed before the conductivity measurements. A known current was applied to the sample and the resultant voltage across the sample was then measured using high precision electrometer (Oriol Instruments). Fig. 8 shows the conductivity variation of MgO thin films as a function of reciprocal temperature for different H^+ ion fluences.

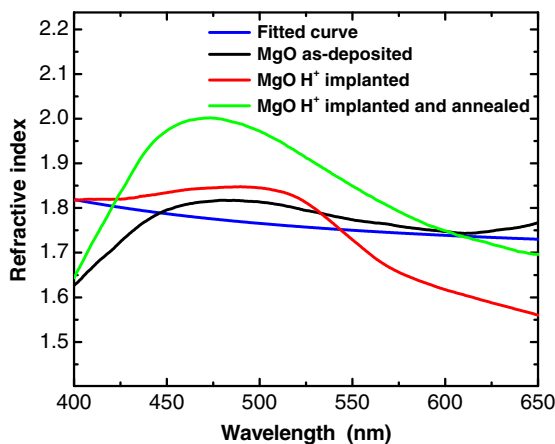


Fig. 7. Variation of refractive index with wavelength for the as-deposited, implanted and post-annealed MgO films.

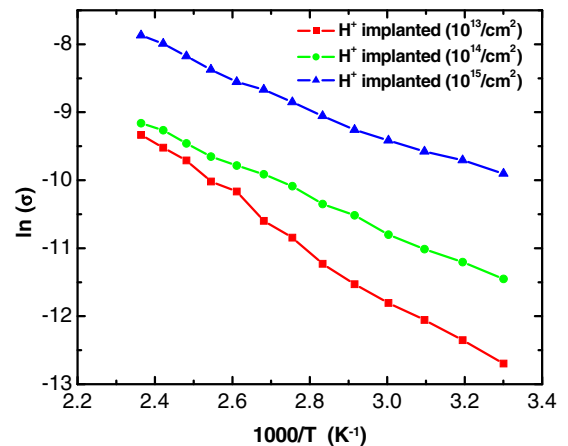


Fig. 8. Conductivity variation of H^+ implanted MgO thin films as a function of reciprocal temperature.

At room temperature, the conductivity increases by about three orders of magnitude for fluences increasing from 10^{13} to 10^{15} ions/cm². At 150 °C, the conductivity increases by about one order from 8.27×10^{-5} S cm⁻¹ to 4.02×10^{-4} S cm⁻¹ for fluences in the range 10^{13} – 10^{15} ions/cm². This indicates that the conductivity is thermally activated in a different manner and the activation energy decreases continuously from 0.53 to 0.27 eV in the same increasing range of fluences. Obtained electrical conductivity is small, when compared to the conductivity of MgO single crystals implanted with Fe⁺ ions to a fluence of 10^{16} – 10^{17} cm⁻² [63]. On iron implantation, the conductivity is increased from 10^{-6} to 10^{-2} S cm⁻¹ in the temperature range 57–227 °C. However, for H⁺ implantations, maximum conductivity is 4.02×10^{-4} S cm⁻¹ at 150 °C. This low conductivity may be due to the implantation fluence, which is less in the present study and also to the nature of ions used.

Normally in implanted crystals, the resistance decreases very rapidly for displacement per atom (dpa) values below 1. Above 1, a saturation is observed and this indicates that the maximum ‘ σ ’ value due to disorder is reached. This happens if all the atoms have been displaced once. In MgO thin films for the fluence of 10^{15} ions/cm², it is noted that the films are not channeling amorphous as was demonstrated by XRD and RBS analysis. The increase in conductivity with fluence is attributed to the increase in the accumulation of lattice defect in the crystal lattice. Also, it is revealed that the temperature dependence conductivity with $\ln(\sigma)$ being proportional to $T^{-1/2}$ and $T^{-1/4}$ and therefore, electron transport occurs through a variable range hopping process in addition to thermal process.

3.5. Surface modification

The AFM micrographs of MgO thin films implanted with H⁺ ions to 10^{15} ions/cm² is shown in Fig. 9. As seen

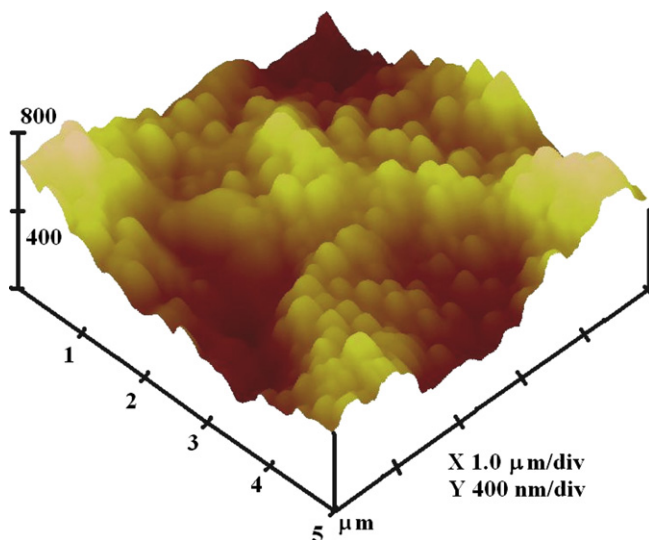


Fig. 9. Surface morphology of MgO thin films implanted with 1.5 MeV H⁺ ions to 10^{15} ions/cm².

in figure, the implantation causes deep as well as shallow pits on the film surface. The implanted ions restrict the uniformity of the columnar growth in the H⁺ implanted samples. Due to the uneven growth in 2D direction, deep and shallow pits are developed. On the other hand, the surface smoothness is spoiled due to the defect clusters. These variations certainly affect the optical and electrical properties and their effects are discussed in the previous sections. However, cavity formation and network dislocations are not visible in the implanted specimens. Complete amorphisation is also not observed as expected from the results of the XRD and RBS studies.

4. Conclusions

The present work has pointed out the effect of hydrogen precipitates embedded in MgO lattice due to H⁺ implantation. The crystalline phase and their modifications due to implantations have been identified with XRD results. A remarkable change in XRD peak intensities and grain size variations are attributed to the decrease in crystallinity as the implantation fluences are increased. The enhanced yield from implanted samples compared to the as-deposited spectrum in Rutherford back scattering spectrometry confirms a mixed damage structure, which probably consists of randomly disordered regions and extended defects. In optical absorption measurements, the most intense band occurred at ~ 5.0 eV had been assigned to the anion vacancies. The extinction of bands observed after thermal annealing indicated the formation and growth of hydrogen colloids. DC electrical measurements of MgO films implanted with hydrogen ions with an energy of 1.5 MeV shows that the electrical conductivity of the implanted area increases with the implantation dosages. This dramatic increase in conductivity is associated with the intrinsic defects induced by the implantation (oxygen vacancies and oxygen interstitials), rather than the implanted H⁺ ions. The electrical conductivity in the implanted area is thermally activated, with activation energy of 0.53–0.27 eV. Surface smoothness of the implanted samples has been altered due to the restricted columnar growth of the grains.

References

- [1] A. van Veen, M.A. van Huis, A.V. Fedorov, H. Schut, F. Labohm, B.J. Kooi, J.Th.M. De Hosson, Nucl. Instr. and Meth. B 191 (2002) 610.
- [2] M. Tardìo, R. Ramírez, R. González, Y. Chen, E. Alves, Nucl. Instr. and Meth. B 191 (2002) 191.
- [3] B. Savoini, D. Cáceres, I. Vergara, R. González, J. Appl. Phys. 95 (2004) 2371.
- [4] M. Lu, C. Lupu, S.M. Lee, J.W. Rabalais, J. Chem. Phys. 115 (2001) 446.
- [5] R.H. Magruder III, L. Yang, R.F. Haglund Jr., C.W. White, L. Yang, R. Dorsinville, I.R. Alfano, Appl. Phys. Lett. 62 (1993) 1730.
- [6] A. Ueda, R. Mu, Y.-S. Tung, M. Wu, W.E. Collins, D.O. Henderson, C.W. White, R.A. Zuhr, J.D. Budai, A. Meldrum, P.W. Wang, X. Li, Nucl. Instr. and Meth. B 141 (1998) 261.

- [7] R.L. Zimmerman, D. Ila, E.K. Williams, S. Sarkisov, D.B. Poker, D.K. Hensley, Nucl. Instr. and Meth. B 141 (1998) 308.
- [8] T. Mitamura, K. Kwatsura, R. Takahashi, T. Adachi, T. Igarashi, S. Arai, N. Masuda, Y. Aoki, S. Yamamoto, K. Narumi, H. Naramoto, Y. Horino, Y. Mokuno, K. Fujii, J. Nucl. Mater. 271–272 (1999) 15.
- [9] M.A. van Huis, A.V. Fedorov, A. van Veen, P.J.M. Smulders, B.J. Kooi, J.Th.M. De Hosson, Nucl. Instr. and Meth. B 166–167 (2000) 225.
- [10] M.L. Knotek, P.J. Feibelman, Surf. Sci. 90 (1979) 78.
- [11] J.C. Bourgoin, J.W. Corgett, J. Chem. Phys. 59 (1973) 4042.
- [12] R. Nagel, A.G. Balogh, Nucl. Instr. and Meth. B 156 (1999) 135.
- [13] M.A. Monge, A.I. Popov, C. Ballesteros, R. González, Y. Chen, E.A. Kotomin, Phys. Rev. B 62 (2000) 9299.
- [14] Y. Qian, D. Ila, R.L. Zimmerman, D.B. Poker, L.A. Boatner, D.K. Hensley, Nucl. Instr. and Meth. B 127–128 (1997) 524.
- [15] R. Kelly, in: O. Anciello, R. Kelly (Eds.), Ion Bombardment Modification of Surfaces, Elsevier, Amsterdam, 1984, p. 79.
- [16] G.H. Kinchin, R.S. Pease, Rep. Prog. Phys. 88 (1955) 1.
- [17] M.J. Norgett, M.T. Robinson, I.M. Torrens, Nucl. Eng. Des. 33 (1975) 50.
- [18] J.P. Biersack, L.G. Haggmark, Nucl. Instr. and Meth. 174 (1980) 257.
- [19] J.F. Ziegler, J.P. Biersack, U. Littmark, The Stopping and Range of Ions in Solids, Pergamon Press, New York, 1985.
- [20] M.A. Monge, A.I. Popov, C. Ballesteros, R. González, Y. Chen, E.A. Kotomin, Phys. Rev. B 62 (2000) 9299.
- [21] R. González, Y. Chen, R.M. Sebeck, G.P. Williams Jr, R.T. Williams, W. Gellermann, Phys. Rev. B 43 (1991) 5228.
- [22] M.A. van Huis, A. van Veen, H. Schut, S.W.H. Eijt1, B.J. Kooi, J.Th.M. De Hosson, T. Hibma, Rev. Adv. Mater. Sci. 4 (2003) 60.
- [23] R. González, I. Vergara, D. Cáceres, Phys. Rev. B 65 (2002) 224108.
- [24] A. Moses Ezhil Raj, L.C. Nehru, M. Jayachandran, C. Sanjeeviraja, Cryst. Res. Technol. 42 (2007) 867.
- [25] R.L. Zimmerman, D. Ila, E.K. Williams, S. Sarkisov, D.B. Poker, D.K. Hensley, Nucl. Instr. and Meth. B 141 (1998) 308.
- [26] J.F.D. Chubaci, S. Watanabe, Nucl. Instr. and Meth. A 280 (1989) 410.
- [27] Joint Commission of Powder Diffraction Data Files, PCPDF WIN, Version 1.30, Pennsylvania, 1997.
- [28] B. E Warren, X-ray Diffraction, Addison Wesley Publishing Co., London, 1969.
- [29] K.L. Chopra, Thin Film Phenomena, McGraw Hill Publishing Company, New York, 1969.
- [30] S. Velumani, Sa.K. Narayanadhas, D. Mangalraj, Semicond. Sci. Technol. 13 (1998) 1016.
- [31] M. Dhanam, R. Balasundar Prabhu, S. Jayakumar, P. Gopalakrishnan, M.D. Kannan, Phys. Status Solidi A 19 (2002) 149.
- [32] A.R. West, Solid State Chemistry and its Applications, John Wiley and Sons, Singapore, 1984.
- [33] B. Savoini, D. Cáceres, I. Vergara, R. González, R.C. da Silva, E. Alves, Y. Chen, J. Appl. Phys. 95 (2004) 2371.
- [34] C. Kittel, Introduction to Solid State Physics, fifth ed., Wiley, New York, 1976.
- [35] C. Aksel, P.D. Warren, F.L. Riley, J. Eur. Ceram. Soc. 24 (2004) 2407.
- [36] W.K. Chu, J.W. Mayer, M.A. Nicolet, Backscattering Spectrometry, Academic Press, New York, 1978.
- [37] L.C. Feldman, J.W. Mayer, S.T. Picraux, Materials Analysis by Ion Channeling: Submicron Crystallography, Academic Press, New York, 1982.
- [38] S.J. Zinkle, S. Kojima, J. Nucl. Mater. 179–181 (1991) 395.
- [39] L. Thomé, J. Fradin, J. Jagielski, A. Gentils, S. Enescu, F. Garrido, Eur. Phys. J. Appl. Phys. 24 (2003) 37.
- [40] S.J. Zinkle, Nucl. Instr. and Meth. B 91 (1994) 234.
- [41] C.J. McHargue, Mater. Sci. Eng. A 253 (1998) 94.
- [42] N. Sasajima, T. Matsui, K. Hojou, S. Furuno, H. Otsu, K. Izui, T. Muromura, Nucl. Instr. and Meth. B 141 (1998) 487.
- [43] L.C. Feldman, J.W. Mayer, S.T. Picraux, Materials Analysis by Ion channeling, Academic Press, New York, 1982.
- [44] J. Jagielski, L. Thomé, L. Nowicki, A. Turos, A. Gentils, F. Garrido, A. Piatkowska, P. Aubert, Nucl. Instr. and Meth. B 240 (2005) 111.
- [45] A.S. Kunsetsov, I.V. Yaek, Sov. Phys.–Solid State 18 (1976) 2051.
- [46] E. Sonder, W.A. Sibley, Point Defects in Solids, Vol. I, Plenum, New York, 1972.
- [47] A. Van Veen, H. Schut, A.V. Fedorov, E.A.C. Neeft, R.J.M. Konings, B.J. Kooi, J.Th.M. de Hosson, Nucl. Instr. and Meth. B 147 (1999) 216.
- [48] B.D. Evans, J. Comas, P.R. Malmberg, Phys. Rev. B 6 (1972) 2453.
- [49] B. Henderson, R.D. Ding, Philos. Mag. 13 (1966) 1149.
- [50] R. Swanepoel, J. Phys. E. Sci. Instrum. 16 (1983) 1214.
- [51] S.H. Wemple, Phys. Rev. B 7 (1973) 3767.
- [52] G.W. Arnold, J. Appl. Phys. 46 (1975) 4466.
- [53] G. Fuchs, G. Abouchacra, M. Treilleux, P. Thevenard, J. Serughetti, Nucl. Instr. and Meth. B 32 (1988) 100.
- [54] G. Abouchacra, G. Chassagne, J. Serughetti, Radiat. Eff. 64 (1982) 189.
- [55] Y. Qian, D. Ila, K.X. He, M. Curley, D.B. Poker, L.A. Boatner, Proc. Mater. Res. Soc. 396 (1996) 423.
- [56] G. Mie, Ann. Phys. 25 (1908) 377.
- [57] W.T. Doyle, Phys. Rev. 111 (1958) 1067.
- [58] A.E. Hughs, S.C. Jian, Adv. Phys. 28 (1979) 717.
- [59] Y. Qian, D. Ila, R.L. Zimmerman, D.B. Poker, L.A. Boatner, D.K. Hensley, Nucl. Instr. and Meth. B 127–128 (1997) 524.
- [60] Y. Dayal, Doctoral dissertation, Illinois Institute of Technology, Chicago, IL, 1965.
- [61] B. Ostle, Statistics in Research, Iowa State University Press, Ames, Iowa, 1954.
- [62] W. Primak, J. Luthsa, Phys. Rev. 150 (1966) 551.
- [63] R. Meaudre, A. Perez, Nucl. Instr. and Meth. B 32 (1988) 75.